

Critical plane analysis of multiaxial fatigue experiments leading to White Etching Crack formation

S Averbeck¹, E Kerscher¹

¹ Materials Testing, University of Kaiserslautern, Gottlieb-Daimler-Strasse, 67663 Kaiserslautern, Germany

stefan.averbeck@mv.uni-kl.de

Abstract. Various researchers have shown that rolling contact fatigue can be reproduced with cyclic compression-torsion experiments, with the load components either in-phase or out of phase. As reported previously, the authors used such experiments to reproduce the rolling contact fatigue phenomenon “White Etching Cracks” which can cause premature failures of rolling element bearings. It is characterized by subsurface crack initiation and propagation coupled with microstructural changes alongside the crack flanks. Surprisingly, only in-phase load superposition caused these microstructural changes to occur. This suggests that White Etching Crack formation is somehow linked to the multiaxial stress state in the specimens, as this was the only variable that changed between in-phase and out-of-phase testing. In this study, the multiaxial stress state in the two experiments is analysed and compared using different critical plane criteria. In contrast to common ways of characterizing the stress state, e.g. equivalent stress approaches, this class of criteria is explicitly designed for multiaxial stress states. Special attention is given to the Dang Van criterion, which has been used in a number of rolling contact fatigue studies.

1. Introduction

White Etching Cracks (WECs) are a premature damage and failure mode found in rolling element bearings across many different industries, bearing manufacturers, and bearing geometries. Due to the important function of bearings and the unpredictability of this damage phenomenon, White Etching Cracks can cause costly secondary damages and downtimes.

WECs are groups or networks of subsurface cracks which are accompanied by zones of microstructurally transformed material [1]. These zones consist of nanocrystalline ferrite with grain sizes of 10-100 nm. Additionally, the primary carbides which are dispersed in the original tempered martensite are dissolved in the transformed areas [2]. In a metallographic analysis, the transformed regions appear white when etched with 3% nitric acid (nital), which explains how WECs get their name.

WEC formation seems to be influenced by a great number of factors, which renders the search for the root causes and mechanisms difficult. The factors can be separated into three main sources: operating conditions (vibration, load peaks, slip), tribochemistry (lubricant composition, water contamination), and surface damage (corrosion, electrical current) [3]. The importance of sliding speed is highlighted by two relatively recent studies proposing characteristic values for WEC formation [4,5]. In terms of mechanisms, two basic directions of thought exist, which explain WEC formation either as hydrogen-induced or stress-induced (both hypotheses are discussed e.g. in [6]). It has also been proposed that both interpretations are correct, and that there are in fact two similar but separate phenomena that are only



summarised under the term “White Etching Cracks” [7]. It should be remembered that while the two approaches emphasise different factors, both generally recognise that the respective other factor also can contribute to WEC formation, and a combined-cause mechanism was proposed by [8].

Investigation of WECs is usually based upon full-scale bearing tests and rolling contact fatigue tests. Several reviews [3,6,9] over the past few years on WEC studies are testimony to the great research activity in this field. In an earlier publication [10], the authors presented a novel experimental approach for reproducing WECs, using cyclic compression-torsion loads on cylindrical specimens. The experiments were based on the observations by other researchers that rolling contact fatigue can be approximated by superimposed compression and torsion, at which both in-phase [11] and out-of-phase loads [12] can be used. In our experiments, it appeared that cracks formed under both load variants; however, WEC-like microstructural transformation in the vicinity of the cracks only occurred during in-phase testing. At the time, we hypothesised that the different stress conditions of the two load cases caused this behaviour, as this was the only parameter that was changed. An exploratory critical plane analysis of the stress conditions suggested that cyclic plasticity processes should be more probable during in-phase testing [13]. In this paper, a more detailed and expanded analysis will be presented. In addition, the Dang Van criterion will be used to analyse the stress conditions in the experiment. As this criterion has been used a number of times in rolling contact fatigue analyses, a comparison between the present results and original RCF cases enables a transfer of the findings from compression-torsion experiments to rolling element bearing conditions.

Table 1. Material properties and testing conditions

Material	
Specification	100Cr6 (AISI 52100, SUJ-2) steel
Yield strength, R_e	1980MPa
Ultimate tensile strength, R_m	2446MPa
Young's modulus, E	208GPa
Hardness	730HV
Testing conditions	
Max. v. Mises equivalent stress	1080MPa
No. of cycles	10^6
Testing frequency	10Hz
Temperature	25°C

2. Methods

The full details of the compression-torsion testing setup can be found in [10] and are summarised in table 1. The most relevant information for this study – the stress values and variation in time of the two stress patterns – is shown in figure 1. In both cases, the compressional and torsional stresses are periodic in time and can be described as a sine wave:

$$[\sigma(t), \tau(t)] = [\sigma_m, \tau_m] + [\sigma_a, \tau_a] \sin(\omega t + \delta) \quad (1)$$

The phase shift δ is zero for all cases except the out-of-phase torsional stress, where it is π . The two load patterns will be referred to as IP (for in-phase) and OP (for out-of-phase) in the following.

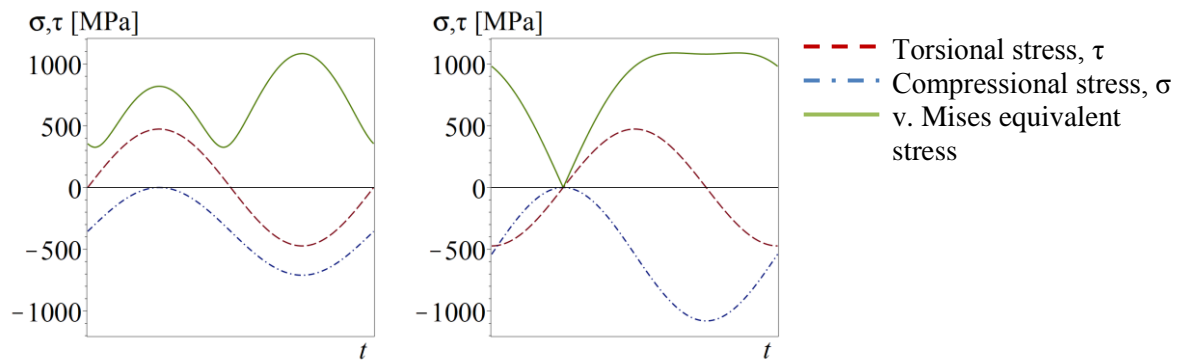


Figure 1. Load variants during testing. Left: in-phase loading, right: 90° out-of-phase loading.

As figure 1 shows, the v. Mises equivalent stress maxima are the same for both load cases, aside from the fact that the maximum equivalent stress acts nearly constantly over a longer portion of the stress cycle in the OP setup. Yet only in-phase loading resulted in WEC-like microstructural changes, which led to the conclusions that a) the stress conditions significantly influence WEC formation and b) that an equivalent stress approach is not suitable to reflect the different stress conditions between the experiments. This is especially true for the effects of phase shifted loads, which generally are more detrimental to the material than in-phase loads [14]. As an alternative means of characterizing the multiaxial stress states, the critical plane approach was chosen.

The common goal of critical plane approaches is to describe multiaxial fatigue better than conventional stress analysis (e.g. equivalent stresses) does, and to predict whether a given multiaxial load can be endured or will lead to failure (for an overview, see [14]). Multiaxial loading causes complex stresses which are highest on certain material planes in the material. These can be described by their orientation angles φ and θ relative to an arbitrary coordinate system xyz (see figure 2). For each plane Δ , a damage parameter can be calculated and compared against a fatigue limit. If the damage parameter exceeds the fatigue limit, fatigue damage will occur, ultimately leading to failure of the specimen or component. The damage parameter and stress limit can be in the form of stresses, strains, or energies.

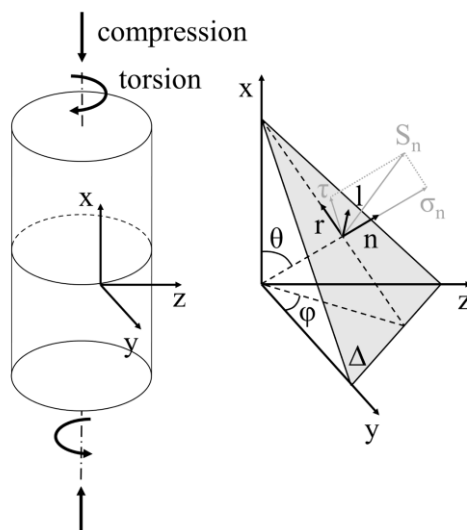


Figure 2. Directions and angles defining the critical plane. Adapted from [15].

For the present evaluation, different stress-based criteria were chosen for the following reasons: 1) The experiments were run in load-controlled mode, so that the macroscopic stresses are clearly defined and their variation over time is well known. 2) The fatigue stress limits of 100Cr6 steel, which is the

steel most frequently used in rolling element bearings, are well documented. Especially relevant for the following are the uniaxial fatigue limit $f_{-1}=650\text{MPa}$ and the torsional fatigue limit $t_{-1}=380\text{MPa}$ (both at a stress ratio of $R=-1$) [16]. In contrast, energy- or strain-based fatigue limits would have to be calculated first-hand, without reference values to compare against. 3) Stress-based criteria were found to yield good results in the high cycle fatigue range (i.e., up to 10^7 load cycles) [14]. This is the relevant fatigue range for the experiments, which were run up to 10^6 cycles.

Within the class of stress-based criteria, the critical plane can be defined as the orientation where a linear combination of the normal and shear stresses amplitudes, N_a and C_a , reaches a maximum:

$$\{\theta^*, \varphi^*\}: \text{Max}(a C_a(\theta, \varphi) + b N_a(\theta, \varphi)) \quad (2)$$

In many cases, a and b are one and zero or vice versa, so that the critical plane orientations θ^* and φ^* are only defined by the normal or shear stress amplitude. Care must be taken to choose an appropriate criterion for a given material, as some are only applicable to certain types of materials (e.g. depending on whether the material is ductile or brittle) [17].

The compression-torsion load case is not very well investigated, and consequently, reference values and even information on the applicability of different criteria are scarce. For this reason, we chose a set of criteria that includes different definitions of the critical plane and the damage parameter. At the same time, the criteria are still similar enough for comparison, so that contradictions and singularities in the results can be identified. The criteria will be presented briefly in the next section. All of them are based on searching for the critical plane(s) caused by the macroscopic stresses. This is in contrast to the Dang Van criterion presented in subsection 2.2, which uses a mesoscopic approach. All calculations were performed using the computer algebra system MAPLE.

2.1. Macroscopic critical plane criteria

It is relatively common for stress-based critical plane criteria to define the critical plane as the plane of maximum shear stress. This definition is based upon the usual failure mode of metallic materials, where shear-controlled failure is most important, except for some very brittle material conditions. As examples of this critical plane definition, the criteria of McDiarmid [18], Matake [19], and Susmel and Lazzarin [20] are used in this study. Differences exist in the respective damage criterion. Both McDiarmid and Matake use a linear combination of shear and normal stresses to determine the critical angles θ^* and φ^* :

$$\sigma_{\text{lim}} \leq C_a(\theta^*, \varphi^*) + \kappa N_{\text{max}}(\theta^*, \varphi^*) \quad (3)$$

C_a is the shear stress amplitude on the critical plane, N_{max} the maximum normal stress perpendicular to the plane. The constant κ is defined as $t_{-1} / 2R_e$ by McDiarmid and $2(t_{-1} / f_{-1}) - 1$ by Matake. Susmel and Lazzarin use a similar but modified criterion, where the maximum normal stress is put in relation to the shear stress amplitude:

$$\sigma_{\text{lim}} \leq C_a(\theta^*, \varphi^*) + \kappa \frac{N_{\text{max}}(\theta^*, \varphi^*)}{C_a(\theta^*, \varphi^*)} \quad (4)$$

In order to keep the dimension MPa, κ in this case is $t_{-1} - 0.5f_{-1}$. Consequently, all three criteria are evaluated against a stress limit, i.e. the fatigue strength of the material at a given number of cycles.

Liu and Mahadevan [17] proposed a criterion using the highest normal stress amplitude, $N_a(\theta^*, \varphi^*)$, as the defining parameter for the critical plane orientation. This criterion was developed specifically with regard to brittle and extremely brittle materials, where normal stresses are failure-critical instead of shear stresses. The damage criterion differs from the other criteria inasmuch as it is dimensionless. It also takes into account the hydrostatic stresses σ_{ha} . The criterion reads

$$\beta \leq \left(\left(\frac{N_a(\theta^*, \varphi^*)}{f_{-1}} \right)^2 + \left(\frac{C_a(\theta^*, \varphi^*)}{t_{-1}} \right)^2 + \kappa \left(\frac{\sigma_{ha}(\theta^*, \varphi^*)}{f_{-1}} \right)^2 \right)^{0.5} \quad (5)$$

The material parameters β and κ can be determined from established fatigue limits. For 100Cr6 steel, κ is zero and β is 0.99. This means that the hydrostatic stress on the critical plane, $\sigma_{ha}(\theta^*, \varphi^*)$, has no influence on the fatigue limit under torsion, which is in agreement with experimental data.

The critical plane definition in the criterion developed by Carpinteri et al. [21] is based on the weighted direction of principal stresses. The endurance limit is formulated as a stress:

$$\sigma_{lim} \leq \left(\left(N_a(\theta^*, \varphi^*) + f_{-1} \frac{N_m}{R_m} \right)^2 + \left(\frac{t_{-1}}{f_{-1}} \right)^2 C_a(\theta^*, \varphi^*)^2 \right)^{0.5} \quad (6)$$

The procedure to calculate the critical plane orientations and stresses is outlined by the authors of each criterion in the cited publications and, more generally, in [22] and [15]. For the application of the general procedure to the specific case of our experiments, see [13]. The shear stress amplitude C_a in particular is not trivial to evaluate, as it is a vector function changing both its direction and value over time and the possible critical plane orientations.

2.2. Dang Van criterion

In addition to the aforementioned five criteria, an analysis with the Dang Van criterion [23] was performed. This criterion has been widely used for rolling contact fatigue analysis, providing reference values for our own results (e.g. [24,25]). One main difference to the criteria cited above is that the scale considered is not macroscopic but mesoscopic. First, the macroscopic stress tensor Σ is split between the hydrostatic part $PH(t)$ and the deviatoric part $S(t)$. In the next step, $S(t)$ is transferred onto the mesoscopic scale, where the mesoscopic stress deviator

$$s(t) = S(t) + \rho^* \quad (7)$$

acts. ρ^* is the mesoscopic residual stress tensor in the stabilised state, which can be calculated as

$$\rho^* = -z : \min_z \left[\max_t \sqrt{(S(t) - z) : S(t) - z} \right] \quad (8)$$

With $s(t)$, the shear stress in Dang Van's criterion

$$\tau_{DV}(t) = \text{Tresca}[s(t)] = \sqrt{s_I(t) - s_{III}(t)} \quad (9)$$

can be calculated and finally, the damage parameter

$$d = \text{Max}_t \left[\frac{\tau_{DV}(t)}{b} - a PH(t) \right] \quad (10)$$

is evaluated over t . If $d \geq 1$, fatigue damage will occur, eventually leading to failure. This general procedure and its theoretical foundations are outlined in more detail in [23] and [26]. For the present case, a simplified evaluation can be used, as all stresses vary periodically in time [24,26]. In contrast to the five criteria described above, searching for the critical plane is not necessary in this criterion. It is implicitly given by the orientation of the principal stresses which are used to calculate $\tau_{DV}(t)$. The endurance domain and load path of a given material and multiaxial load can be visualised in a diagram like figure 3.

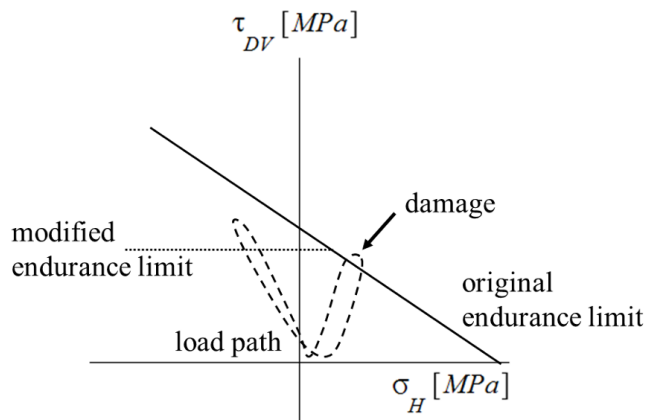


Figure 3. Endurance domain and an exemplary load path in the Dang Van criterion (adapted from [23])

Since its first publication, the criterion has been refined and extended to better cover the real behaviour of materials. In its first form, the criterion predicted an increasing shear fatigue limit when negative (i.e. compressive) hydrostatic stresses are applied [23]. Finding that this disagrees with experimental observations, Desimone et al. [25] proposed a modified fatigue limit composed of two segments with different slopes, as shown by the dotted line in figure 3. They noted that this leads to a conservative estimation, as the fatigue limit for pure torsion is outside the endurance domain; yet, if compressive hydrostatic stresses occur during the stress history, which is invariably the case in rolling contact fatigue, the modified curve better predicts fatigue behaviour. Further refinement of the endurance limit especially for compressive hydrostatic stresses may be necessary. For example, there is experimental evidence that the endurance limit actually decreases as the hydrostatic stresses increase [24]. As these results were obtained for rail steel, which is in many ways different from bearing steels, the constant endurance limit will be used in this study.

Another benefit of using the modified limit is that, for the present case, no exact knowledge of the residual stresses in the material is necessary. At the surface of both bearing rings and the specimens used in this study, compressive residual stresses can be expected from the final stages of the manufacturing process, namely grinding and polishing [27]. These stresses, however, have only the effect of moving the load path further into the region of compressive hydrostatic stresses (i.e., to the left in figure 3) [25]. This does not affect the endurance limit, so that macroscopic residual stresses can, as a first approximation, be ignored.

3. Results

3.1. Macroscopic critical plane criteria

The different definitions of the critical plane lead to different predictions regarding the orientations of critical planes. As the McDiarmid, Matake, and Susmel-Lazzarin criterion all define the critical plane as the plane of highest shear stress amplitude, their predicted critical orientations coincide with the global maxima of figure 4a, which shows the evaluation of $C_a(\theta, \varphi)$ for the in-phase load. The diagrams are periodic in θ and φ , as adding multiples of π to the angles result in the same planar orientation, only with alternating normal vectors. The location of the OP maxima is slightly offset by 0.06π along the φ axis. The Liu-Mahadevan criterion, using the normal stress amplitude to determine the critical planes, predicts very different angles of φ , as shown in figure 4b. Again, the OP case has its maxima slightly shifted along the φ axis, this time by 0.02π . The variation over θ is the same for both IP and OP, with maxima of equal height at 0.5π and 1.5π . It is therefore sufficient to conduct an analysis of the influence of φ on the damage parameters at constant $\theta = (j+0.5)\pi$, with $j=0,1,2,\dots,n$. Consequently, the following diagrams will be only two-dimensional.

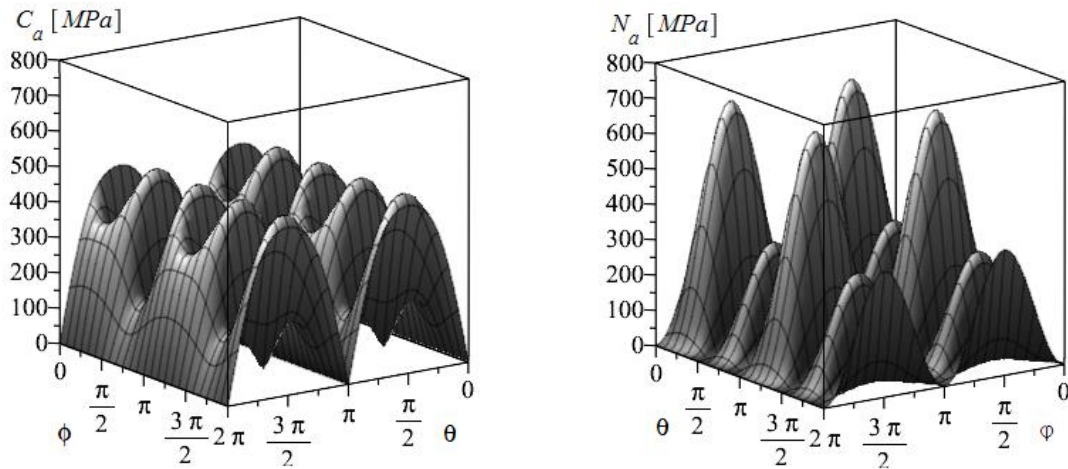


Figure 4. Shear stress amplitude (left) and normal stress amplitude (right) under IP load.

As figure 4 shows, the criteria using C_a to define the critical planes predict a higher number of critical orientations. The Carpinteri-Spagnoli criterion has a unique critical plane definition, using the weighted principal stresses. This leads to a single critical plane at $\theta=0.5\pi$, $\phi=0.44\pi$.

When evaluating the damage parameter of the criteria by Matake, McDiarmid, and Susmel and Lazzarin, one finds that the predicted critical plane orientations do not always correspond to global maxima of the damage parameter. In the Matake criterion, this behaviour is less pronounced for IP load (figure 5a), where the values of the global and local maxima are very close to each other, than for OP load (figure 5b), where distinct global maxima exist. In both cases, all maxima stay below the uniaxial fatigue limit of 650MPa, which corresponds to none of the specimens having failed during 10^6 cycles. The torsional fatigue limit of 380MPa is exceeded on a number of orientations; however, this is not the limit that critical plane criteria are usually compared against.

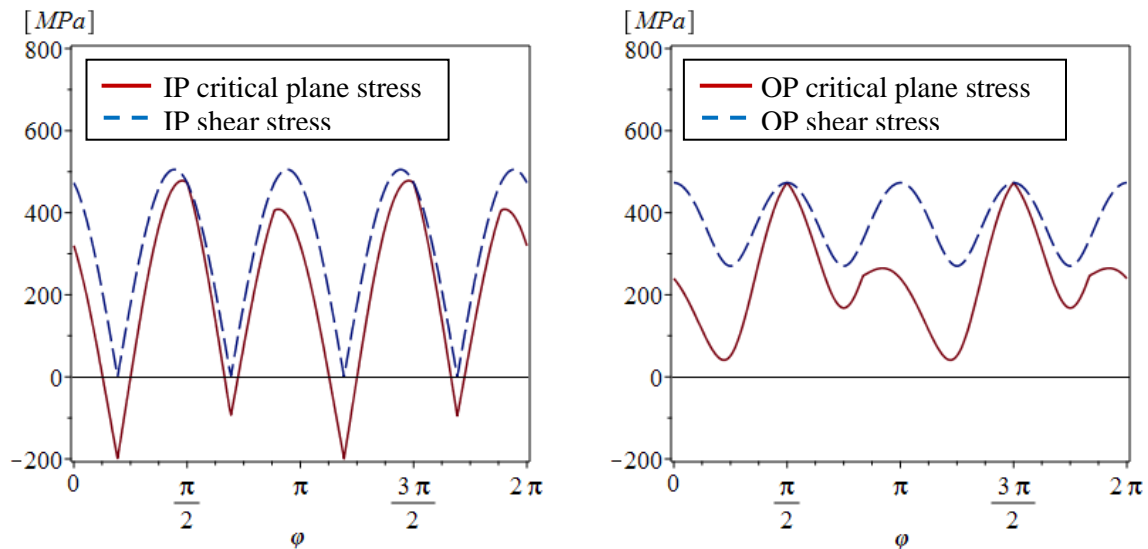


Figure 5. Damage parameter of the Matake criterion for IP (left) and OP load (right). The shear stress amplitude C_a for both cases is also shown.

In addition to the damage parameter curve, the evolution of the shear stress amplitude C_a is shown in figure 5. Comparing the location of the maxima of the damage parameter among the ϕ axis with the critical orientations predicted by C_a , a small but noticeable shift between the two can be observed. From

the basic definition of the critical plane as the plane experiencing the highest stresses, one would expect the two to coincide. The difference can be traced to the contribution of N_{\max} to the damage parameter. As the evolution of N_{\max} over φ does not coincide with that of C_a , the linear combination $C_a + \kappa N_{\max}$ will have its maxima shifted compared to C_a . The same behaviour is found in the McDiarmid criterion, the results of which are overall similar enough to figure 5 that a separate diagram is omitted.

The criterion by Susmel and Lazzarin has distinct singularities at $\varphi = [0.23\pi, 0.77\pi, 1.23\pi, 1.77\pi]$ in the in-phase case, where very high negative values are found (see figure 6). The absolute values at these orientations exceed realistic stresses by several orders of magnitude. An explanation for this behaviour can be found in the second term of the criterion. When $N_a > N_m$ and $C_a < 1$, the expression $(-N_a + N_m)/C_a$ assumes very high negative values and with the other summand C_a being negligibly small in this case, the singularities occur. The orientations and damage parameter values of the critical planes remain unaffected by this and are very similar to the previous results. Likewise, the prediction that in-phase loads will generate a higher number of critical orientations than out-of-phase loads stands as in the previous two criteria, and again a discrepancy between the predicted and the actual critical orientations is observed (figure 6).

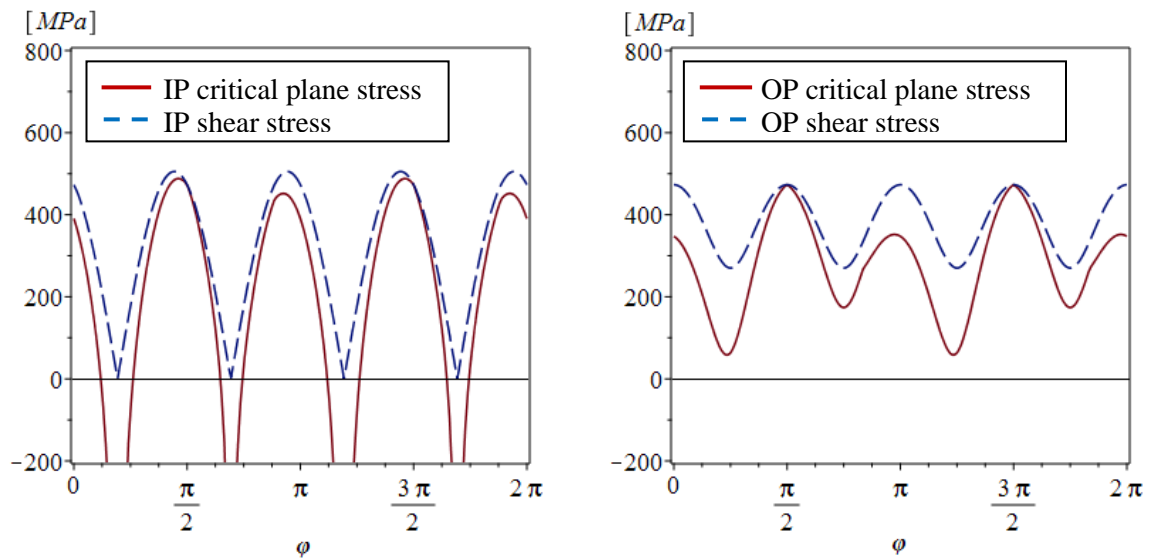


Figure 6. Damage parameter of the Susmel-Lazzarin criterion for IP (left) and OP load (right).

The shear stress amplitude C_a for both cases is also shown.

Results for the Liu-Mahadevan criterion are presented in figure 7. As discussed above, determining the critical planes via the normal load amplitude leads to very different predictions regarding the orientation of the critical planes. Comparing these predicted values with the location of the actual maxima of the damage parameter, one finds a much more pronounced discrepancy between the two. This is especially true in the IP case, where the global maxima of N_a correspond to local minima of the damage parameter. The resulting difference between the predicted and the actual critical orientation is 0.25π . Moreover, the stress distribution is much more uniform than it would be expected from the N_a curve. Another major difference is that the damage parameter is above the endurance limit of $\beta=0.99$ for most orientations. This is not in agreement with the experimental data, as none of the specimens failed during testing.

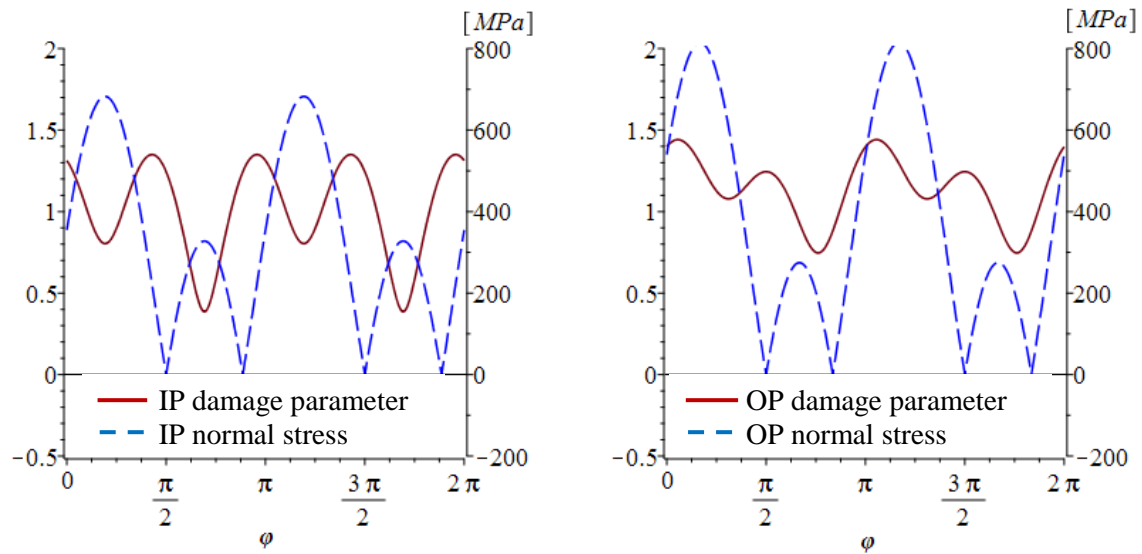


Figure 7. Damage parameter of the Liu-Mahadevan criterion for IP (left) and OP load (right). The normal stress amplitude N_a for both cases is also shown.

The Carpinteri-Spagnoli criterion, due to its critical plane definition via the principal stress directions, results in only one predicted critical orientation. Therefore, the diagram in figure 8 is different from figures 5-7, showing only the graphs of the damage parameter for IP and OP load. The critical angles θ^* remain at $(j+0.5)\pi, j=0,1,2,\dots,n$, which is the same as for all other criteria. The prediction for φ^* is close to the real value in the OP case, where only a difference of 0.04π is found. In the IP case, meanwhile, the difference is much greater at 0.11π . Secondary maxima are found at $\varphi=(j+0.96)\pi$ which reach almost the same damage parameter value as the global maxima. Generally, the stresses on the critical planes are significantly higher (+60% at the in-phase maxima, +100% at the out-of-phase maxima), exceeding the uniaxial fatigue limit on most orientations just like the Liu-Mahadevan criterion.

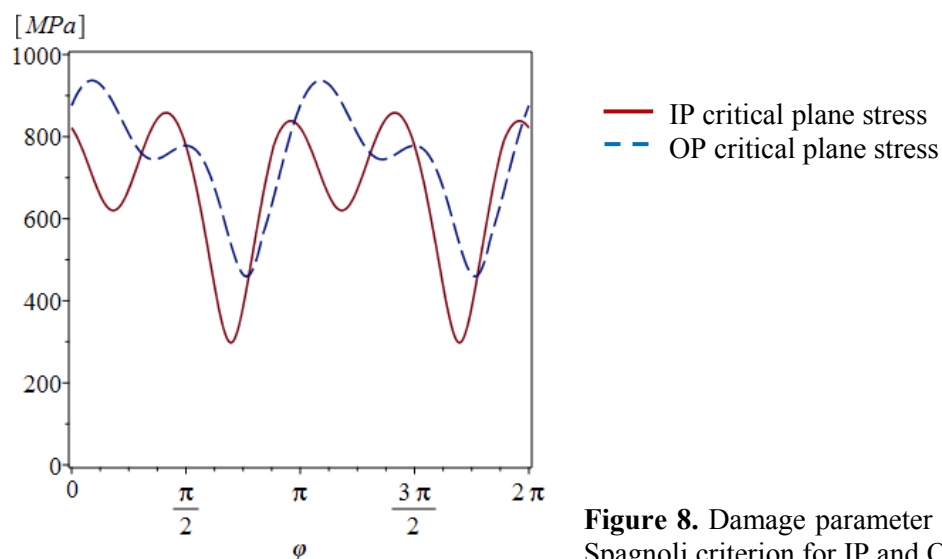


Figure 8. Damage parameter of the Carpinteri-Spagnoli criterion for IP and OP load.

Table 2 shows a comparison of the discrepancies between predicted and real critical plane orientation encountered in the different criteria. Only the plane of highest damage parameter value is shown. To all

stated orientations, multiples of π can be added for equivalent orientations. For the shear stress-based critical plane definition, the shift is limited to less than 10%. Likewise, the underestimation of the stresses on the critical plane is of the same magnitude and is usually small enough to be negligible. The Liu-Mahadevan criterion is the notable exception, with significant differences between predicted at real value in both load cases. The orientation difference is up to 0.25π . In the IP case, the damage parameter on the predicted critical plane is almost 40% less than on the actual critical plane. Finally, the Carpinteri-Spagnoli criterion achieves good results in the OP case but underestimates the critical plane stresses in the IP case.

Table 2: Differences between predicted and real values for the orientation of the critical plane and the maximum damage parameter

Criterion	Critical plane angle φ		Maximum damage parameter value	
	As defined	Real	On definitional critical plane	On real critical plane
Matake				
IP	0.44π	0.48π	462.1MPa	478.0MPa
OP	0.50π	0.50π	473.0MPa	473.0MPa
McDiarmid				
IP	0.44π	0.46π	481.0MPa	486.7MPa
OP	0.50π	0.50π	473.0MPa	473.0MPa
Susmel and Lazzarin				
IP	0.44π	0.46π	483.5MPa	488.2MPa
OP	0.50π	0.50π	473.0MPa	473.0MPa
Liu and Mahadevan				
IP	0.19π	0.43π	0.83^a	1.36^a
OP	0.17π	0.09π	1.59^a	1.67^a
Carpinteri et al.				
IP	0.52π	0.41π	737.5MPa	858.2MPa
OP	0.05π	0.09π	925.2MPa	936.8MPa

^a Dimensionless damage parameter

3.2. Dang Van criterion (mesoscopic scale)

The general stress tensor for the two load cases in this paper is (cf. [24])

$$\boldsymbol{\sigma} = \begin{bmatrix} \sigma_m + \sigma_a \sin(\omega t) & \tau_a \sin(\omega t) & 0 \\ \tau_a \sin(\omega t) & 0 & 0 \\ 0 & 0 & 0 \end{bmatrix} \quad (11)$$

The resulting residual stress tensor is

$$\boldsymbol{\rho}^* = \begin{bmatrix} -\frac{2}{3}\sigma_m & 0 & 0 \\ 0 & \frac{\sigma_m}{3} & 0 \\ 0 & 0 & \frac{\sigma_m}{3} \end{bmatrix} \quad (12)$$

which leads to a mesoscopic stress deviator of the form

$$\hat{s}(t) = \begin{bmatrix} \frac{2}{3}\sigma_a \sin(\omega t) & \tau_a \sin(\omega t + \delta) & 0 \\ \tau_a \sin(\omega t + \delta) & -\frac{\sigma_a}{3} \sin(\omega t) & 0 \\ 0 & 0 & -\frac{\sigma_a}{3} \sin(\omega t) \end{bmatrix} \quad (13)$$

The hydrostatic stress is

$$PH(t) = \frac{\sigma_m}{3} + \frac{\sigma_a}{3} \sin(\omega t) \quad (14)$$

and the Dang Van shear stress is

$$\tau_{DV}(t) = 0.5 \sqrt{(\sigma_a \sin(\omega t))^2 + 4(\tau_a \sin(\omega t))^2} \quad (15)$$

With the last two equations, the load path at the critical orientation can be drawn in a diagram like figure 3 for both load variants, as depicted in figure 9. The modified endurance limit is also shown.

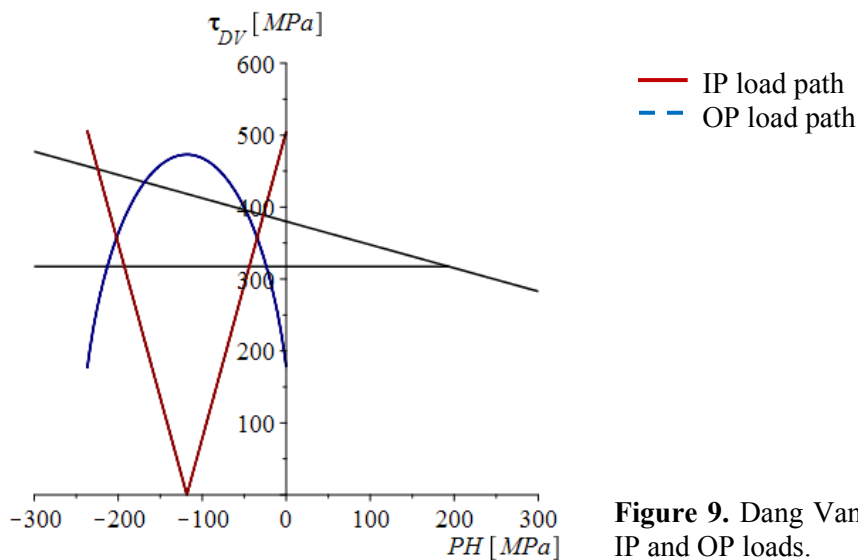


Figure 9. Dang Van criterion. Load paths for IP and OP loads.

The exact position of the load curves along the compressive stress axis cannot be determined without information on the residual stresses present in the material. However, as discussed in section 2.2, the compressive residual stresses that are likely to be present in the specimens would only effect a translation towards higher negative hydrostatic stresses, meaning that the portion of the curve beyond the endurance limit remains unaffected for the modified endurance domain.

This limitation notwithstanding, the Dang Van criterion correctly predicts that fatigue damage will occur in both cases, as parts of both load paths are beyond the endurance limit. It should be noted that surpassing the endurance limit of this criterion only means that crack initiation rather than failure will occur [23]. The load paths themselves are very different. The IP curve consists of two straight lines meeting at the x-axis. This point is the instant of zero torsional stress. Only the minor portion of one load cycle is spent beyond the endurance limit, but the shear stress maxima are fairly high. The OP curve is a parabola with its maximum at slightly lower shear stresses than in the IP case. The shear stresses are over the endurance limit during a greater part of the OP cycle and never reach the value zero. One major difference is that the IP shear stresses are highest at the extreme points of hydrostatic stress, while the shear stress maximum of the OP load is achieved in the presence of moderate compressive stresses.

For both load paths, comparable curves can be found in rolling contact studies by other authors. The in-phase curve resembles, for example, the ones shown in [23]. The out-of-phase curve is similar to the curves in [24].

It is important to notice one fundamental difference between the Dang Van criterion and the five multiaxial fatigue criteria presented above. In the latter, we were concerned with the variation of the damage parameter over different *orientations*, whereas figure 9 shows the variation in *time*. The critical orientation(s) of the Dang Van criterion can be determined from the principal stresses, as they are used in the calculation of $\tau_{DV}(t)$ in equation (9). For the two load cases discussed here, the critical orientations are $\theta^*=(j+0.5)\pi, j=0,1,2,\dots,n$ for both load cases. In the OP case, $\varphi^*=j\pi$ and in the IP case, $\varphi^*=(j+0.5)\pi$.

4. Discussion

It might be appropriate to begin discussing the results by remembering that the present analysis is of a somewhat experimental nature. One could say that it repurposes critical plane criteria, which were originally developed to predict component lifetime under multiaxial fatigue loads. This aspect is of little concern for the present study, as the underlying experiments were run well below the failure limit. The actual goal is to understand the stress conditions and processes in the material leading to the microstructural changes (especially grain refinement) that are typical for White Etching Cracks. In this context, any circumstances influencing the mobility of dislocations are of particular interest. The reason for this is that we suppose WEC formation to be controlled by a mechanism similar to those responsible for nanograin formation in very high cycle fatigue [28] and severe plastic deformation [29]. In both of these cases, the formation of dislocation cells leads to sub-grain formation and ultimately to a grain refinement compared to the original structure. Naturally, drawing conclusions on grain-scale mechanisms based on macroscopic critical plane criteria risks a too high degree of simplification. However, there might still be some useful insights to be gained from a better characterization of the multiaxial stress state compared to other approaches such as equivalent stresses or stress intensity factors. Considering this background, the Dang Van criterion offers perhaps the greatest potential, as its mesoscopic approach is well suited for a grain-level interpretation.

From the macroscopic criteria, it seems that the shear stress amplitude is a better determinant of the critical planes than the normal stress amplitude. The criteria by Matake, McDiarmid, and Susmel-Lazzarin predict the local and global stress maxima with good accuracy. This is especially important in the IP load case, where the local maxima of the damage parameter are almost as high as the global maxima. For the original use of critical plane criteria, i.e. lifetime prediction, this is (at least in a first approximation) of no great relevance, as the highest load determines lifetime. For the present study, these secondary critical planes are important, as their presence indicates that dislocation movement should generally be easier in the IP than in the OP case. However, too many moving dislocations of similar orientation can block each other's movement. In this context, it is interesting to note that the three abovementioned criteria also predict steeper gradients of the damage parameter for IP. This could mean that the IP load case strikes a favourable balance between dislocation mobility on certain planes and inactive dislocations on others, while the OP load activates too few slide systems to cause significant rearrangement. However, due to the very high dislocation density in hardened bearing steels, conclusions on this subject are difficult. In high carbon steels like 100Cr6, the influence of carbon on dislocation mobility must also be considered.

In order to further validate the criteria, we plan to relate the critical plane orientations with the growth direction of the fatigue cracks found on the specimens. With the present results, this is not yet possible, as the critical plane and the actual crack plane are not necessarily the same [30]; however, several methods for calculating the fracture plane do exist [17].

The discrepancies between predicted and real critical orientation are rather high for the criterion by Liu and Mahadevan. This may seem surprising, as the criterion was developed especially for brittle materials, which hardened steel would usually be assumed to be. Yet, bearing applications require sufficient toughness in addition to high hardness. Tempering treatment and residual austenite content of bearing steel could mean that this material is still brittle when compared to other metals but not brittle in the

sense of the criterion (although the fatigue strength ratio of 100Cr6 is within the range for which the criterion is defined). The criterion also predicts failure of the specimens under both load variants, which is not in agreement with experimental evidence. It is conceivable that the high compressive, i.e. negative normal stresses pose a problem in the applicability of the criterion. Little information is available on this subject, as compression-torsion studies based on critical plane criteria are scarce.

The Carpinteri-Spagnoli criterion accurately predicts the orientation of the most critical plane for the OP case. However, like the Liu-Mahadevan criterion, it tends to give too conservative a lifetime estimation under the investigated loads. In the IP case, the critical plane angle φ^* and the critical plane stresses are not predicted correctly. For this study in particular, there is the added problem that only one critical plane orientation is found, which means that the secondary maxima can be overseen.

This last criticism can also be levelled at the mesoscopic Dang Van criterion. Its formulation with the Tresca equivalent stress, which in turn is based on the principal stresses, means that only one, namely the most critical, orientation will be identified. The criterion still is a valuable addition for studying the stress conditions induced by the two load patterns, as it provides information on the stress variation on the critical plane over time. Studying the markedly different load paths of one IP and OP cycle and comparing them with examples from other rolling contact fatigue studies opens opportunities for a better understanding of the differences between the load variants. At a first glance, it is surprising that two load patterns leading to markedly different multiaxial stress states can both be used to recreate rolling contact fatigue conditions. However, the stress field in a Hertzian contact is complex and depends both on time and the observed location. It is probable that the two load variants correspond to different points in the Hertzian contact. If this is the case, the region that is critical for WEC formation could be pinpointed. Unfortunately, the references used to compare the two Dang Van load paths seldom state the exact location leading to one or the other shape; further investigation is necessary on this subject.

5. Conclusion

The stress conditions of two cyclic compression-torsion load patterns used in White Etching Crack reproduction experiments were analysed using five stress-based macroscopic critical plane criteria and the mesoscopic Dang Van criterion. This approach repurposes critical plane criteria, which were developed for lifetime prediction, and continues earlier work to make critical plane criteria useful for the study of WECs. It was found that of the criteria studied, those which define the critical plane as the plane on which the highest shear stress amplitude occurs yielded the most useful results. The findings are interpreted as to their significance for dislocation mobility and dislocation cell formation.

The normal stress amplitude is found to be not a good indicator of critical plane orientations for both compression-torsion load cases. In addition, the lifetime estimation of the criterion is very conservative, predicting failure where none occurred during the experiments. This was also true for the Carpinteri-Spagnoli criterion, which, while very accurately predicting the critical plane in the OP case, underestimates lifetime and does not point to planes on which the damage parameter is close but not equal to the global maximum, especially for the IP load.

The Dang Van criterion is a valuable addition to the criteria based on shear stress amplitude. While it can only be used to search for the plane of the highest stresses, it shows the evolution of the stresses on this plane over time. A comparison of the load paths representing the experimental loads leads to the assumption that the load variants represent different locations and/or instants of a Hertzian contact. Further work should focus on correlating the predicted fracture orientations of different criteria to the crack angles found in tested specimens.

Acknowledgements

We gratefully acknowledge financial support by the German Research Foundation (Deutsche Forschungsgemeinschaft, DFG) under grant KE1426/6-1.

References

- [1] Kotzalas M N and Doll G L 2010 *Phil. Trans. R. Soc. A* **368** 4829–50
- [2] West O, Diederichs A M, Alimadadi H, Dahl K V and Somers M 2013 *Pract. Metallogr.* **50** 410–31
- [3] Evans M-H 2012 *Tribol. Int.* **28** 3–22
- [4] Ruellan Du Crehu, Arnaud 2014 *Tribological Analysis of White Etching Crack (WEC) Failures in Rolling Element Bearings* Ph.D. thesis (INSA Lyon: Lyon)
- [5] Loos J 2014 Einfluss der Reibbeanspruchung auf die WEC-Bildung in Wälzlager 55. *GfT-Tagung* (Göttingen) chapter 23 pp 1-13
- [6] Stadler K, Lai J and Vegter R H 2014 A review: The dilemma with premature white etching crack (WEC) bearing failures *Bearing Steel Technologies* ed Beswick J M (West Conshohocken: ASTM International) pp 487–508
- [7] Alberdi A and Gomez R 2016 Typical bearing damage modes in wind turbines *Proc. Lubmat 2016 Conf.* (Bilbao, Spain)
- [8] Gegner J 2011 Tribological aspects of rolling bearing failures *Tribology - Lubricants and Lubrication* ed Kuo C-H (Rijeka: InTech) pp 33–93
- [9] Evans M-H 2016 *Mater. Sci. Technol.* **32** 1133–69
- [10] Averbeck S and Kerscher E 2016 *Frattura ed Integrità Strutturale* **38** 12–8
- [11] Burkart K, Bomas H, Schroeder R and Zoch H-W 2012 Rolling contact and compression-torsion fatigue of 52100 steel with special regard to carbide distribution *Bearing Steel Technologies* ed Beswick J M (West Conshohocken: ASTM International) pp 218–36.
- [12] Beretta S and Foletti S 2012 Propagation of small cracks under RCF: a challenge to multiaxial fatigue criteria *Proc. of the 4th Int. Conf. on Crack Paths (CP 2012)* ed Carpinteri A et al. (Cassino: Gruppo Italiano Frattura) pp 15–28
- [13] Averbeck S and Kerscher E 2016 *Eng. Fract. Mech. (Preprint j.engfracmech.2016.12.011)*
- [14] Fatemi A and Shamsaei N 2011 *Int. J. Fatigue* **33** 948–58
- [15] Papadopoulos I V 1998 *Fatigue Fract. Eng. M.* **21** 269–85
- [16] Gabelli A, Lai J, Lund T, Rydén K, Strandell I and Morales-Espejel G E 2012 *Int. J. Fatigue* **38** 169–80
- [17] Liu Y and Mahadavan S 2005 *Int. J. Fatigue* **27** 790–800
- [18] McDiarmid D L 1991 *Fatigue Fract. Eng. M.* **14** 429–53
- [19] Mataka T 1977 *Bulletin of JSME* **20** 257–63
- [20] Susmel L and Lazzarin P 2002 *Fatigue Fract. Eng. M.* **25** 63–78
- [21] Carpinteri A, Spagnoli A and Vantadori S 2011 *Int. J. Fatigue* **33** 969–76
- [22] Papadopoulos I V 1997 *Int. J. Fatigue* **19** 219–35
- [23] Dang Van K, Griveau B and Message O 1989 On a new multiaxial fatigue limit criterion: theory and application *Biaxial and Multiaxial Fatigue* ed Brown M W and Miller K J (London: Mechanical Engineering Publications) pp 479–96
- [24] Bernasconi A, Filippini M, Foletti S and Vaudo D 2006 *Int. J. Fatigue* **28** 663–72
- [25] Desimone H, Bernasconi A and Beretta S 2006 *Wear* **260** 567–72
- [26] Dang Van K, Cailletaud G, Flavenot J F, Le Douaron A and Lieurade H P 1989 Criterion for high cycle fatigue failure under multiaxial loading *Biaxial and Multiaxial Fatigue (EGF 3)* ed Brown M W and Miller K J (London: Mechanical Engineering Publications) pp 459–78
- [27] Bhadeshia H 2012 *Prog. Mater. Sci.* **57** 268–435
- [28] Grad P, Reuscher B, Brodyanski A, Kopnarski M and Kerscher E 2012 *Scr. Mater.* **67** 838–41
- [29] Estrin Y and Vinogradov A 2013 *Acta Mater.* **61** 782–817
- [30] Karolczuk A and Macha E 2005 *Int. J. Fract.* **134** 267–304